IEEE Photonics Journal
An IEEE Photonics Society Publication

Open Access

Enhanced Performance of Perovskite Light-Emitting Devices With Improved Perovskite Crystallization

Volume 9, Number 1, February 2017

Yue-Feng Liu
Yi-Fan Zhang
Ming Xu
Zhen-Yu Zhang
Jifang Tao
Yuandong Gu
Jing Feng
Hong-Bo Sun, *Member, IEEE*

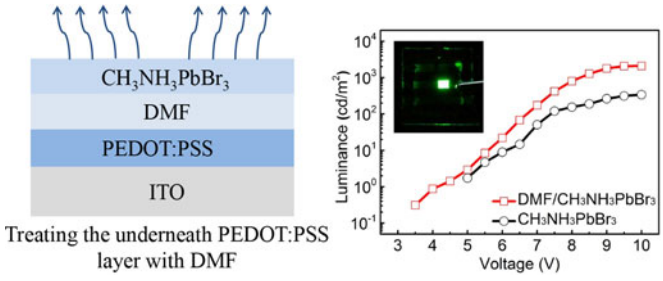

DOI: 10.1109/JPHOT.2016.2647204
1943-0655 © 2017 IEEE

Enhanced Performance of Perovskite Light-Emitting Devices With Improved Perovskite Crystallization

Yue-Feng Liu,[1] Yi-Fan Zhang,[1] Ming Xu,[1] Zhen-Yu Zhang,[1] Jifang Tao,[2] Yuandong Gu,[2] Jing Feng,[1] and Hong-Bo Sun,[1] *Member, IEEE*

[1]State Key Laboratory on Integrated Optoelectronics, College of Electronic Science and Engineering, Jilin University, Changchun 130012, China
[2]Agency of Science Technology and Research, Singapore 138634

DOI:10.1109/JPHOT.2016.2647204

Manuscript received November 8, 2016; revised December 23, 2016; accepted December 28, 2016. Date of publication January 4, 2017; date of current version January 19, 2017. This work was supported in part by the National Natural Science Foundation of China under Grant 61505065, Grant 61675085, Grant 61322402, Grant 61605056, and Grant 61590930. Corresponding author: Jing Feng (e-mail: jingfeng@jlu.edu.cn).

Abstract: In this paper, we have demonstrated an efficient perovskite light-emitting device (PeLED) by improving perovskite crystallization. The improved perovskite crystallization has been achieved by pretreating the underneath poly (3, 4-ethylenedioxythiophene): poly(styrenesulfonate) (PEDOT: PSS) layer with N, N-dimethylformamide (DMF) solvent before single-step spin-coating the perovskite, which results in a prolonged wet environment during the perovskite thermal annealing process to promote the grain growth. The improved perovskite crystallization induces a perovskite thin film with higher surface coverage, fewer defects, and larger grain size with less scattering of grain boundaries. As a result, the PeLEDs exhibit maximum external quantum efficiency of 0.728% and maximum luminance of 2088 cd/m^2, which represent a significant improvement over the control devices. Moreover, perovskite films with improved crystalline quality have proved its beneficial effect on the device stability.

Index Terms: Light-emitting diodes (LEDs), optoelectronic materials, sources.

1. Introduction

Organic-Inorganic hybrid perovskite materials have attracted much attention due to their easy solution process, and they require no high-temperature and tunable optical bandgap in the visible to infrared regions. It will be a fascinating material for applications in low-cost and large-area optoelectronic devices [1]–[6]. Recent work on high-efficiency methylammonium lead trihalide perovskite photovoltaics has shown these materials to possess not only high charge-carrier mobility, mechanical and thermal stability of inorganic semiconductors but also flexibility, simple processing, facile tuning of optical and electrical properties of organic semiconductors [7]–[9]. Recently, bright and color tunable electroluminescence (EL) devices with perovskite materials were reported. It is shown that excellent emission properties of perovskite, such as a narrow full width at half maximum and high photoluminescence quantum yield, and indicates these materials will generally be applicable in display and lighting [6], [10], [11].

The EL properties of the perovskite light-emitting devices (PeLEDs) are influenced strongly by the morphology and quality of methylammonium lead trihalide perovskite thin film. One-step deposition [12], [13], two-step sequential deposition [14], [15], and vapor deposition [16], [17] have been developed to produce high-quality perovskite films. In PeLEDs, the simplicity of the one-step solution deposition approach makes it preferable to other methods due to potential fabrication cost reduction. However, low perovskite film coverage on flat substrates in the simple one-step spin-coating and defects in perovskite crystalline grain result in modest performance of the PeLEDs. Therefore, it is important to optimize the film quality to obtain superior device performance in PeLEDs using the one-step deposition method.

In this paper, the performances of PeLEDs have been enhanced by improving the quality of the perovskite films. A simple method for improved $CH_3NH_3PbBr_3$ crystallites on poly (3, 4-ethylenedioxythiophene): poly(styrenesulfonate) (PEDOT: PSS) layer has been used, which provide a prolonged wet environment during the perovskite thermal annealing to promote grain growth by treating with N, N-dimethylformamide (DMF) before single-step perovskite spin-coating. As a result, perovskite thin films with higher surface coverage, fewer defects and larger grain size with less scattering of grain boundaries were obtained. These improvements of perovskite film quality contribute to the enhanced performance of the PeLEDs at room temperature. Moreover, the improved quality of perovskite film is beneficial to the stability of the device.

2. Experimental Details

2.1 Fabrication of $CH_3NH_3PbBr_3$ Perovskite Films

Fig. 1(a) is a schematic illustration of the formation method for improved crystallized perovskite thin films. The perovskite precursor solution was prepared by mixing CH_3NH_3Br (99.5%, Xi'an polymer light technology corp) and $PbBr_2$ (99.99%, obtained from Xi'an polymer light technology corp) in a 3:1 molar ratio in anhydrous DMF with a concentration of 5 wt% to give a perovskite film thickness of $\sim$20 nm. The patterned ITO substrates were pre-cleaned with acetone, alcohol, and deionized water. The PEDOT: PSS films were prepared by spin coating the PEDOT: PSS aqueous solution (Clevios P VP AI 4083) on glass substrates at 3500 rpm for 30 s. Then the PEDOT: PSS films were dried at 150 °C for 10 min on a hot plate. DMF was spin coated onto the PEDOT: PSS film at 3000 rpm for 30 s, then $CH_3NH_3PbBr_3$ precursor solution was immediately dropped and spin coated at 3000 rpm for 30 s. For the control devices, $CH_3NH_3PbBr_3$ precursor solution was directly spin coated on the PEDOT: PSS/ITO substrate at 3000 rpm for 30 s without the pre-treatment of the DMF. Finally, the $CH_3NH_3PbBr_3$ precursor film was gradually dried at 100 °C for 15 min by further evaporation of solvent for inducing the crystallization of $CH_3NH_3PbBr_3$ perovskite. All steps were operated inside a nitrogen-filled glovebox. The morphology of $CH_3NH_3PbBr_3$ perovskite thin film on PEDOT: PSS/ITO substrate with and without the DMF pre-treatment were investigated by the scanning electron microscope (SEM, JEOL JSM-7500F) and the atomic force microscopy (AFM, iCON, Veeko). The X-ray diffraction (XRD) of the perovskite thin films were characterized by a Rigaku X-ray diffractometer. Absorption spectra measurements were performed by a Shimadzu UV-2550 spectrophotometer and the emission spectrum were measured by a Hitachi F-4600 fluorescence spectrophotometer. Time-resolved PL spectra was performed by time-correlated single-photon counting (TCSPC). Transient absorption spectroscopy was obtained by femtosecond time-resolved pump-probe technology.

2.2 Fabrication and Characterization of PeLEDs

The PeLEDs with and without the DMF pre-treatment were both fabricated. After the fabrication of the perovskite film, the substrates were transferred into thermal evaporation chamber. Then, the organic layers and top contact were deposited layer by layer at a rate of 1 Å s^{-1} and at a base pressure of 5×10^{-4} Pa. Poly (9, 9-dioctylfluorene) (F8) has been used as a charge-blocking layer in perovskite LEDs in previous works. However, redundant blue emission from F8

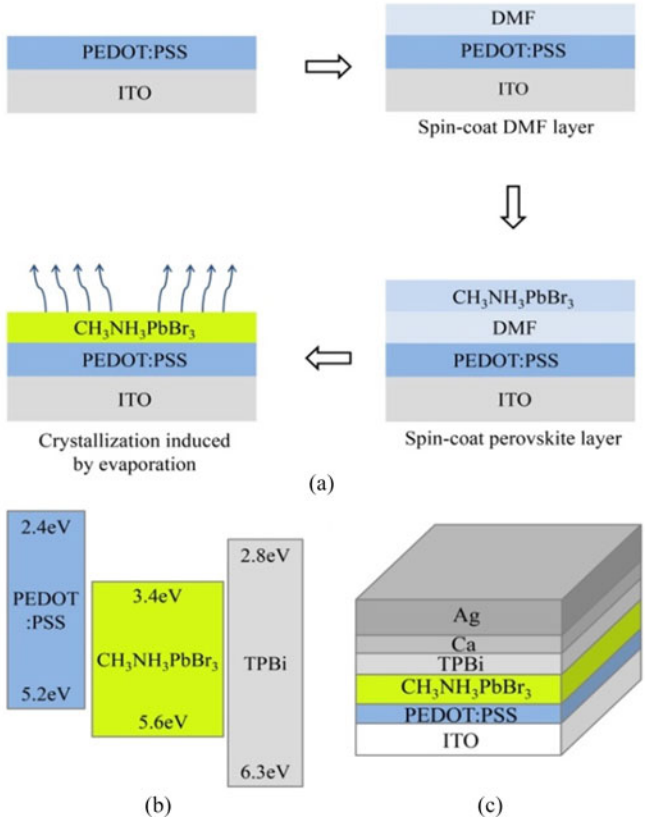

Fig. 1. (a) Schematic illustration of the formation method for improved crystallites perovskite films. (b) Energy-level diagram of PEDOT: PSS/ $CH_3NH_3PbBr_3$/TPBi and (c) stacked structure of the PeLEDs.

reduces the color purity [11], [18]. To ensure color purity of PeLEDs, we use 1, 3, 5-tris (1-phenyl-1H-benzimidazol-2-yl) benzene (TPBi) to replace F8. TPBi can effectively transport electron and block injected holes with an appropriate lowest unoccupied molecular orbital (LUMO, 2.8 eV) and a deep highest occupied molecular orbital (HOMO, 6.3 eV) [19] [see Fig. 1(b)]. The low work function calcium electrode provides ohmic electron injection, while the high work function PEDOT: PSS acts as the hole-injection layer. The structure of our device is ITO/PEDOT: PSS/ CH3NH_3PbBr_3/TPBi(35 nm)/Ca(3 nm)/Ag(80 nm), as shown in Fig. 1(c). The active area of the device is 2 $\times$ 2 mm^2. The voltage–luminance and voltage–current density characteristics of the devices were measured by Keithley 2400 programmable voltage–current source and photo research PR-655 spectrophotometer. All of the measurements were conducted in air at room temperature.

3. Results and Discussion

Generally, the crystallization process comprises of nucleation and growth stages wherein growth depends on the evaporation of solvent. Pre-treatment of DMF before spin coating $CH_3NH_3PbBr_3$ precursor solution prolongs the evaporation time of solvent through increasing the content of the solvent without increasing the concentration of the $CH_3NH_3PbBr_3$ solution. Since both $PbBr_2$ and CH_3NH_3Br have high solubility in DMF, DMF pre-treatment can maintain a prolonged wet environment so that the precursor ions and molecules can diffuse a longer distance during the thermal annealing process compared to that without the DMF pre-treatment, which promotes the grain growth and enhances the surface coverage of perovskite film. Therefore, improved $CH_3NH_3PbBr_3$ perovskite crystallites layer with DMF pre-treatment on the PEDOT: PSS/ITO substrate will be formed.

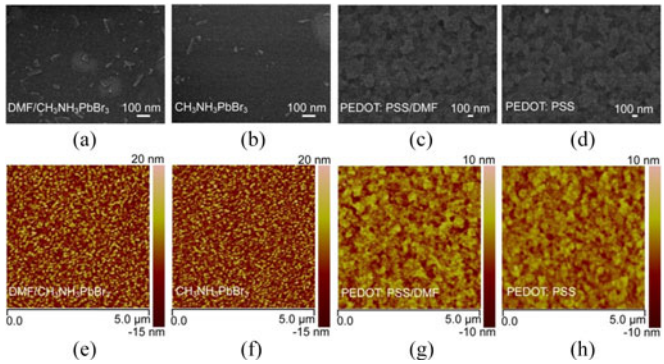

Fig. 2. (a)–(d) SEM and (e)–(h) AFM images of $CH_3NH_3PbBr_3$ perovskite films and PEDOT: PSS films (a), (c), (e), (g) with and (b), (d), (f), (h) without the DMF pre-treatment.

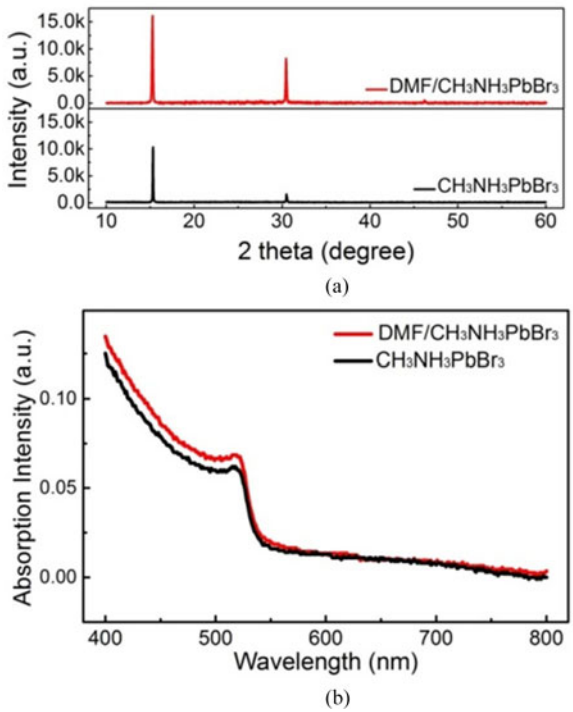

Fig. 3. (a) XRD patterns and (b) absorption spectra of $CH_3NH_3PbBr_3$ perovskite thin films with and without the DMF pre-treatment.

The top-view SEM and AFM images of $CH_3NH_3PbBr_3$ films and PEDOT: PSS films with and without the DMF pre-treatment are shown in Fig. 2. As expected, the $CH_3NH_3PbBr_3$ perovskite film with DMF pre-treatment has higher surface coverage of perovskite film. It showed larger grain density and meant the improvement of the surface coverage. Meanwhile, the grain sizes of the perovskite crystal are increased. The average grain sizes formed with and without the DMF pre-treatment are about 45.52 nm and 34.97 nm, respectively. These considerable differences produced by the two deposition processes show that the DMF pre-treatment is effective to improve $CH_3NH_3PbBr_3$ perovskite thin-films. Moreover, the PEDOT: PSS films with and without DMF almost showed identical surface morphologies and indicated that the DMF pre-treatment has not brought influence on the PEDOT: PSS films. The XRD patterns of the above two films are compared and shown in Fig. 3(a). The XRD pattern of the $CH_3NH_3PbBr_3$ film shows sharp diffraction peaks at 15.28° for the (100) plane and 30.46° for (200). It is confirmed that the XRD data obtained for our $CH_3NH_3PbBr_3$ films

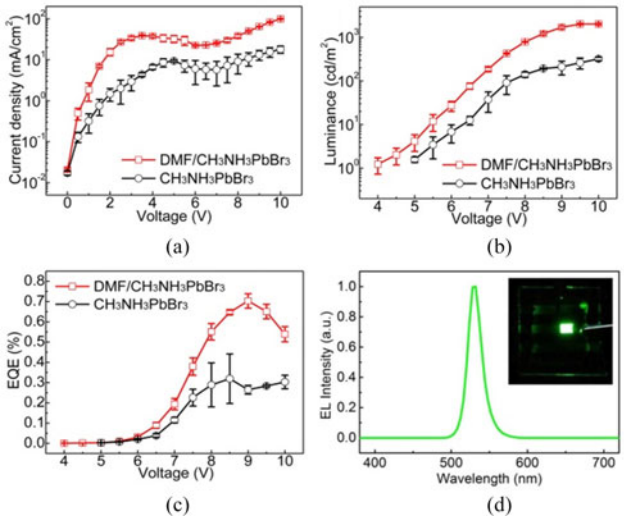

Fig. 4. (a) Current density versus voltage characteristics. (b) Luminance versus voltage characteristics. (c) External quantum efficiency versus voltage characteristics of perovskite light-emitting devices with and without the DMF pre-treatment. (d) Normalized EL spectra and photograph (inset) of $CH_3NH_3PbBr_3$ PeLEDs with the DMF pre-treatment driven at 10 V.

yield the same results as those in the literature based on a comparison of the XRD spectral results [20]. The intensity of the peak diffracted by the (100) plane in the XRD spectra of the $CH_3NH_3PbBr_3$ film with the DMF pre-treatment is improved by 155% compared with that of the $CH_3NH_3PbBr_3$ without the DMF pre-treatment. Intense XRD signal observed for the crystalline $CH_3NH_3PbBr_3$ films identifies enhanced crystallinity with fewer defects and larger grain size with less scattering of grain boundaries. Fig. 3(b) shows the absorption spectra of the two films. The absorption spectra of both films exhibit a typical feature of a perovskite material with band gap energy 2.38 eV, in good agreement with previous reports. The absorption peak is located at 520 nm corresponding to the direct band gap transition from the valence band (VB) to the conduction band (CB). The spectrum of the perovskite films with the DMF pre-treatment shows a higher absorbance, and this implies that the films have better crystallites and lattices which are consistent with the XRD results.

The EL performances of the PeLEDs with or without the DMF pre-treatment are examined. Both current density and luminance are much more enhanced for PeLEDs with the DMF pre-treatment as can be seen in Fig. 4(a) and (b). The PeLEDs without the DMF pre-treatment exhibit a maximum luminance of 340.6 cd/m^2 at 10 V. While, the PeLEDs with the improved quality of perovskite films exhibit a remarkably improved maximum luminance of 2088 cd/m^2 at 10 V. Fig. 4(c) shows the external quantum efficiency (EQE) of the devices. The EQE were calculated by employing MATLAB according to the following equation [21] due to PeLEDs with ITO anode can be regarded as Lambertian:

$$\eta_{ext} = \frac{\pi e L_v(0)}{K_m h c J} \frac{\int \lambda P(\lambda)\, d\lambda}{\int V(\lambda) P(\lambda)\, d\lambda}$$

where e, Km, h, c, J, Lv(0), P(λ), and V(λ) are, respectively, the quantity of an electron charge, a conversion constant, Planck constant, velocity of light in vacuum, current density, spectral luminance at 0°, relative spectral power distribution of the device at 0°, and the normalized photopic spectral response function. The device with the DMF pre-treatment shows an obvious increase in quantum efficiency. The maximum EQE reaches up to 0.728%, while it is 0.405% for the control device. The EL spectrum of the PeLEDs at 10V applied bias is shown in Fig. 4(d). The emission peak of the $CH_3NH_3PbBr_3$ perovskite LED is located at 528 nm and the FWHM of the emission is approximately 20 nm. There are no additional emission peaks in the EL spectrum. The using of the TPBi allows the PeLEDs to satisfy their potential as color-pure and stable devices with sharp emission spectra,

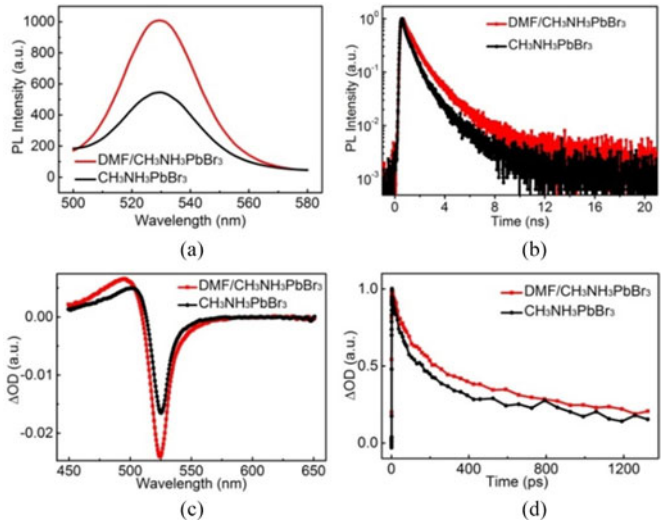

Fig. 5. (a) PL intensities, (b) PL lifetime curves, (c) transient absorption spectra, and (d) Kinetic profiles of 400 nm transient bleach recovery of $CH_3NH_3PbBr_3$ perovskite films with and without the DMF pre-treatment.

because TPBi has a deep valence band at 6.3 eV and presents a barrier of 0.7 eV to that of the perovskite [see Fig. 1(b)]. As shown in the inset of Fig. 4(d), EL from the device is uniform across the entire device pixel with no sign of nonhomogeneity, proving that the emission of perovskite nanocrystals is uniformly distributed across the spin-coated film.

The enhanced performances of $CH_3NH_3PbBr_3$ perovskite film by the DMF pre-treatment arise from higher coverage, higher crystallinity, fewer defects and larger grain size. As we know, the diffusion length of excitons or charge carriers is increased with the increased size of the perovskite grains, which promote the exciton dissociation into carriers. However, in our case, the perovskite film formed by 5 wt% perovskite precursor solution is thin enough ($\sim$20 nm) to spatially confine effect to make electrons and holes for bimolecular recombination. The grain size of perovskite produced with the DMF pre-treatment is just slightly increased, so that the negative influence of larger grain size to the bimolecular recombination is negligible. Meanwhile, the increased crystallinity with fewer internal and surface defects and larger grain size with less grain boundaries can efficiently suppress nonradiative recombination and improve radiative recombination. In addition, enhanced coverage also can promote exciton formation in perovskite film and the number of excitons can be increased. These factors result in the enhanced EL performance of the PeLEDs.

Carrier recombination lifetimes measured by photoluminescence (PL) are commonly taken as a property of perovskite film quality. The films with longer decay lifetimes were considered as better-performing materials. We conducted steady-state and time-resolved (tr-PL) PL measurements on the samples of glass/PEDOT: PSS/$CH_3NH_3PbBr_3$ with or without the DMF pre-treatment. The PL of $CH_3NH_3PbBr_3$ perovskite peaking at 529 nm [Fig. 5(a)] appears slightly redshift compared with the EL. The PL intensity of the sample with the DMF pre-treatment increases obviously, which implies better lattice formed. Fig. 5(b) shows the tr-PL dynamics of the aforementioned samples. The measured tr-PL decays are fitted with a stretched exponential function to obtain the respective PL lifetimes. The lifetime for the perovskite film without the DMF pre-treatment is about 1.05 ns. As the crystallite quality is improved by the DMF pre-treatment, an increased lifetime of about 2.5 ns is observed, which is beneficial to the light emission performance of the devices. Moreover, to clarify the inter-band transitions on an ultrafast timescale and explore deeper insight into the dynamics of photogenerated free charges in $CH_3NH_3PbBr_3$ films, femtosecond transient absorption spectroscopy has been measured. Under excitation wavelength of 400 nm, intense photoinduced bleaches arise corresponding to these transitions. The transient absorption spectra (pumped with intensity at 9.2 μJ cm^{-2}) in Fig. 5(c) shows ground bleaching signal at 525 nm ($\sim$2.36 eV), which is

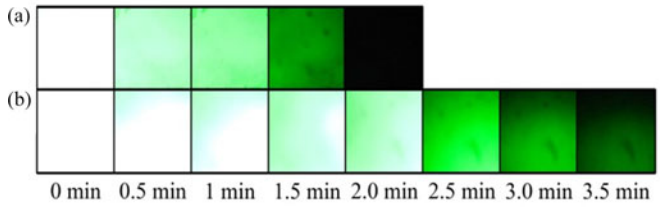

Fig. 6. Operating $CH_3NH_3PbBr_3$ PeLEDs (a) without and (b) with the DMF pre-treatment at different time.

approximately equal to the band gap energy. With the DMF pre-treatment, stronger photoinduced bleaches of $CH_3NH_3PbBr_3$ films arise corresponding to the transition, which is consistent with the trend of the PL intensity. The normalized bleaching kinetics for the samples is shown in Fig. 5(d). In the control sample, the carriers recombine with an initial time constant of approximately 86 ps. In contrast, the sample with the DMF pre-treatment shows a much longer decay with an initial time constant of approximately 108 ps. The increased PL lifetime and transient decay time further confirm the fewer defect densities and less grain boundaries in the improved crystallites perovskite film induced by the DMF pre-treatment.

The effect of the improved perovskite crystallization on the stability of the PeLEDs is investigated. Photographs of the operating devices at different time with and without crystallization are shown in Fig. 6. The unencapsulated devices which were fabricated simultaneously were operated in air atmosphere at room temperature. The driving current for operating devices is 12.5 mA/cm^2. It is obvious that the luminance of the device without the DMF pre-treatment exhibits more quickly decay. The device decays completely after 2 min operation. While in case of the device with the DMF pre-treatment, homogeneous luminance can be still observed even after 2 min and severe decay appear after 3.5 min. These results show that perovskite film with improved crystalline quality effectively improve the stability of the PeLEDs.

4. Conclusion

In summary, enhanced performance of the PeLEDs by improving the quality of the perovskite crystals have been demonstrated. The pre-treating of the underneath PEDOT:PSS layer with DMF before single-step spin-coating of the perovskite promotes the perovskite crystallinity by prolonging the wet environment during the perovskite thermal annealing. The improved perovskite crystallization result in a perovskite thin film with higher surface coverage, fewer defects and larger grain size with less scattering of grain boundaries. As a result, the PeLEDs have shown a maximum EQE of 0.728% and a maximum luminance of 2088 cd/m^2. Moreover, the perovskite film with the improved perovskite crystallization is beneficial to the stability of the PeLEDs. This work has provided a simple strategy to simultaneously improve the luminance, efficiency, and stability of the PeLEDs.

References

[1] H. S. Kim *et al.*, "Lead iodide perovskite sensitized all-solid-state submicron thin film mesoscopic solar cell with efficiency exceeding 9%," *Sci. Rep.*, vol. 2, 2012, Art. no. 591.
[2] M. H. Kumar *et al.*, "Flexible, low-temperature, solution processed ZnO-based perovskite solid state solar cells," *Chem. Commun.*, vol. 49, pp. 11089–11091, 2013.
[3] A. Mei *et al.*, "A hole-conductor-free, fully printable mesoscopic perovskite solar cell with high stability," *Science*, vol. 345, pp. 295–298, 2014.
[4] Y. Rong *et al.*, "Solvent engineering towards controlled grain growth in perovskite planar heterojunction solar cells," *Nanoscale*, vol. 7, pp. 10595–10599, 2015.
[5] J. H. Kim *et al.*, "High-performance and environmentally stable planar heterojunction perovskite solar cells based on a solution-processed copper-doped nickel oxide hole-transporting layer," *Adv. Mater.*, vol. 27, pp. 695–701, 2015.
[6] G. Xing *et al.*, "Low-temperature solution-processed wavelength-tunable perovskites for lasing," *Nature Mater.*, vol. 13, pp. 476–480, 2014.

[7] J. M. Ball, M. M. Lee, A. Hey, and H. J. Snaith, "Low-temperature processed meso-superstructured to thin-film perovskite solar cells," *Energy Environ. Sci.*, vol. 6, pp. 1739–1743, 2013.
[8] P. Docampo *et al.*, "Solution deposition-conversion for planar heterojunction mixed halide perovskite solar cells," *Adv. Energy Mater.*, vol. 4, pp. 1400355-1–1400355-6, 2014.
[9] D. Liu and T. L. Kelly, "Perovskite solar cells with a planar heterojunction structure prepared using room-temperature solution processing techniques," *Nature Photon.*, vol. 8, pp. 133–138, 2013.
[10] F. Deschler *et al.*, "High photoluminescence efficiency and optically pumped lasing in solution-processed mixed halide perovskite semiconductors," *J. Phys. Chem. Lett.*, vol. 5, pp. 1421–1426, 2014.
[11] Z. K. Tan *et al.*, "Bright light-emitting diodes based on organometal halide perovskite," *Nature Nanotech.*, vol. 9, pp. 687–692, 2014.
[12] G. E. Eperon, V. M. Burlakov, P. Docampo, A. Goriely, and H. J. Snaith, "Morphological control for high performance, solution-processed planar heterojunction perovskite solar cells," *Adv. Funct. Mater.*, vol. 24, pp. 151–157, 2014.
[13] N. J. Jeon, J. H. Noh, Y. C. Kim, W. S. Yang, S. Ryu, and S. I. Seok, "Solvent engineering for high-performance inorganic-organic hybrid perovskite solar cells," *Nature Mater.*, vol. 13, pp. 897–903, 2014.
[14] D. Liu, M. K. Gangishetty, and T. L. Kelly, "Effect of CH3NH3PbI3 thickness on device efficiency in planar heterojunction perovskite solar cells," *J. Mater. Chem. A*, vol. 2, pp. 19873–19881, 2014.
[15] J. Burschka *et al.*, "Sequential deposition as a route to high-performance perovskite-sensitized solar cells," *Nature*, vol. 499, pp. 316–319, 2013.
[16] M. Liu, M. B. Johnston, and H. J. Snaith, "Efficient planar heterojunction perovskite solar cells by vapour deposition," *Nature*, vol. 501, pp. 395–398, 2013.
[17] O. Malinkiewicz *et al.*, "Metal-oxide-free methylammonium lead iodide Perovskite-based solar cells: The influence of organic charge transport layers," *Adv. Energy Mater.*, vol. 4, pp. 1400345-1–1400345-9, 2014.
[18] G. Li *et al.*, "Efficient light-emitting diodes based on nanocrystalline perovskite in a dielectric polymer matrix," *Nano Lett.*, vol. 15, pp. 2640–2644, 2015.
[19] J. W. Kim *et al.*, "Study of sequential dexter energy transfer in high efficient phosphorescent white organic light-emitting diodes with single emissive layer," *Sci. Rep.*, vol. 4, 2014, Art. no. 7009.
[20] E. Edri, S. Kirmayer, M. Kulbak, G. Hodes, and D. Cahen, "Chloride inclusion and hole transport material doping to improve methyl ammonium lead bromide Perovskite-based high open-circuit voltage solar cells," *J. Phys. Chem. Lett.*, vol. 5, pp. 429–433, 2014.
[21] F. Ma *et al.*, "Model and simulation on the efficiencies of microcavity OLEDs," *Opt. Commun.* vol. 285, pp. 3100–3103, 2012.